Analysis and simulation of static Kramer drive under steady-state conditions

B.A.T. Al Zahawi, BSc, PhD
B.L. Jones, BSc(Eng), PhD, CEng, MIEE
W. Drury, BSc, PhD, CEng, MIEE

Indexing terms: Power electronics

Abstract: A rigorous analysis of the static Kramer drive under steady-state conditions is described in which stator variables are transformed on to a frame of reference which is stationary with respect to the rotor. For constant-speed operation the system equations are reduced to a set of linear differential equations with constant coefficients which are solved to predict drive waveforms, allowing for inverter DC-voltage waveform, DC-link-current ripple and the changing states of conduction of the rotor rectifier diodes. Eigenvalue and eigenvector techniques are applied to obtain analytical expressions which greatly reduce computation time. The harmonic content of the various current waveforms is examined, and the analysis used to examine certain features of drive performance such as stator-current pulsations at certain speeds. Results were verified experimentally and display very good agreement with measurement.

List of symbols

f	= AC supply frequency
s	= p.u. slip
ω	= AC-supply angular frequency
ω_r	= shaft angular velocity
L_d	= DC-link inductance
R_d	= DC-link resistance
i_d, I_d	= instantaneous and mean DC-link current
v_d, V_d	= instantaneous and mean rectifier DC voltage
v_i, V_i	= instantaneous and mean inverter DC voltage
α	= thyristor firing-delay angle
$(1:N)$	= recovery-transformer primary/secondary voltage ratio
V_w	= RMS stator phase-winding voltage
v_{AB}, v_{BC}, v_{CA}	= instantaneous supply line-to-line voltages
v_{AS}, v_{BS}, v_{CS}	= instantaneous supply line-to-neutral voltages
V_f, R_f	= diode threshold voltage and slope resistance
V_t, R_t	= thyristor threshold voltage and slope resistance
$R_1, X_1, R_c, X_m, X'_2, R'_2$	= motor equivalent-circuit parameters
$(1:n)$	= stator/rotor turns ratio
v_A, v_B, v_C	= instantaneous stator phase voltages
v_a, v_b, v_c	= instantaneous rotor phase voltages
i_A, i_B, i_C	= instantaneous stator phase currents
i_a, i_b, i_c	= instantaneous rotor phase currents
R_s, R_r	= stator and rotor phase-winding resistances
$\underline{L}_s, \underline{L}_r$	= stator and rotor phase-winding self-inductances
$\underline{M}_s$	= mutual inductance between stator phase windings
$\underline{M}_r$	= mutual inductance between rotor phase windings
$\underline{M}$	= maximum value of mutual inductance between a stator and a rotor phase winding
L_s	$= \underline{L}_s - \underline{M}_s$
L_r	$= \underline{L}_r - \underline{M}_r$
M	$= \sqrt{(3/2)}\underline{M}$
$\theta_1, \theta_2, \theta_3$	= angular displacements between the axes of stator phase A and rotor phases a, b and c
v_Γ, v_Δ	= transformed stator voltages
i_Γ, i_Δ	= transformed stator currents

Paper 6903B (P1/6), first received 5th May 1989

Dr. Al Zahawi is with Cortina Electric Co. Ltd., Tolpits Lane, Watford WD1 8XL, United Kingdom

Dr. Jones is with RMCS (Cranfield), Shrivenham, Swindon SN6 8LA, United Kingdom

Dr. Drury is with NEI Control Systems Ltd., Team Valley, Gateshead NE11 0QJ, United Kingdom

1 Introduction

The usual form of the static Kramer drive, shown in Fig. 1, is based on a wound-rotor induction motor with a

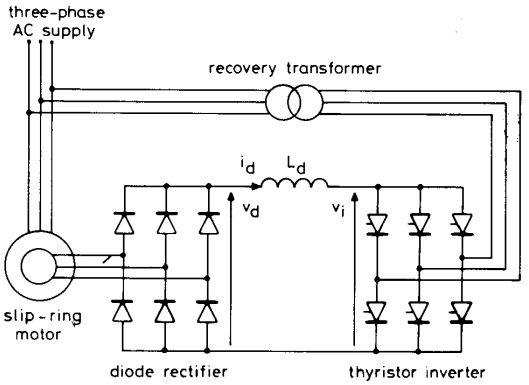

Fig. 1 *Static Kramer drive*

slip-energy recovery circuit which comprises a diode rectifier and a line-commutated inverter connected to the AC supply, via a step-up transformer when the stator voltage is higher than the rotor voltage. A smoothing reactor L_d is normally connected between rectifier and inverter.

Slip power is returned to the mains via the inverter, thus providing a simple and efficient form of AC variable-speed drive which is of special interest for pumps, fans and other loads whose torque is proportional to the square of the speed. In such applications, control is often needed over a limited speed range below synchronous speed, allowing substantial reductions in diode and thyristor costs and in the reactive power and harmonic currents drawn from the supply.

The mean rectifier output voltage V_d, approximately proportional to slip, is countered by the inverter back EMF whose mean value V_i is controlled by the inverter firing-delay angle α, where normally $90° < \alpha < 180°$. The stator is fed at fixed voltages and frequency, giving almost constant airgap flux and a torque which is approximately proportional to mean DC-link current I_d. Motor speed can therefore be adjusted by changing α, yielding similar torque/speed characteristics and control requirements to those for a separately excited DC motor.

The simplicity of the drive itself contrasts with the complexity of its performance analysis, due to the interdependence between rectifier conduction states and the inevitably nonsinusoidal rotor waveforms. A rigorous analysis should take account of not only the mutual coupling between rotor and stator coils, between rotor coils and between stator coils, but also the inverter input-voltage waveform and consequential DC-link-current ripple.

The literature includes several useful papers where all these points have been addressed. Giannakopoulos and Galanos [1] numerically integrated the system differential equations and accounted for the effects of rectifier- and inverter-switching operation. Franz and Meyer [2] performed a similar analysis of a drive with a 6/12-pulse recovery system.

Huber [3] identified the different rotor states resulting from rectifier switching and transformed machine equations on to a frame of reference which is stationary with respect to the rotor, but his equations retained the angular displacement between stator and rotor axes as a variable. This variable was eliminated in the analysis performed by Brown, Drury, Jones and Vas [4] where the transformation of machine equations retained the natural rotor variables to determine diode-conduction states, but transformed the stator variables on to a frame of reference stationary with respect to the rotor, thus eliminating time-varying functions of rotor angle. Rotor voltage and current constraints were introduced to simplify the system equations to a set of linear differential equations with constant coefficients which were then solved numerically.

It is shown in this paper how, for constant-speed conditions, matrix and eigenvalue techniques can be applied to obtain analytical expressions for stator and rotor quantities, instantaneous torque, power, etc. greatly reducing the number of time-consuming numerical calculations needed.

The analysis has been verified by experiment and the discrete Fourier transform employed to obtain the harmonic spectrum of drive-current waveforms. Some of the effects of machine-current harmonics, for example the phenomena of instantaneous-torque fluctuations and pulsating supply and stator currents at certain speeds, have been investigated.

The main simplifying assumptions are that AC-supply impedance, and hence inverter-commutation overlap, is negligible, as are motor saturation, core losses and space harmonics.

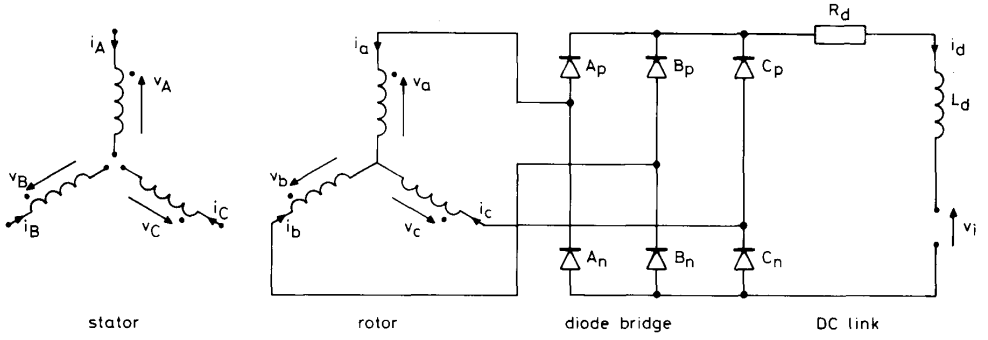

Fig. 2 *Simplified circuit used for analysis*

2 Machine-voltage equations and transformations

The essential features of the system are represented in Fig. 2. The flux linkage for each winding can be expressed as the sum of the flux linkages due to each individual current. Therefore, for the six-winding slip-ring machine, there are six voltage equations in which the voltage is a function of all six currents. These equations are given in matrix form in eqn. 1 which is the familiar voltage equation of the three-phase *ABCabc* slip-ring machine in the 'natural' frame of reference, i.e. the stator reference frame is fixed to the stator and the rotor reference frame to the rotor.

$$\begin{bmatrix} v_A \\ v_B \\ v_C \\ v_a \\ v_b \\ v_c \end{bmatrix} = \begin{bmatrix} R_s + \underline{L}_s p & \underline{M}_s p & \underline{M}_s p & \underline{M}p\cos\theta_1 & \underline{M}p\cos\theta_2 & \underline{M}p\cos\theta_3 \\ \underline{M}_s p & R_s + \underline{L}_s p & \underline{M}_s p & \underline{M}p\cos\theta_3 & \underline{M}p\cos\theta_1 & \underline{M}p\cos\theta_2 \\ \underline{M}_s p & \underline{M}_s p & R_s + \underline{L}_s p & \underline{M}p\cos\theta_2 & \underline{M}p\cos\theta_3 & \underline{M}p\cos\theta_1 \\ \underline{M}p\cos\theta_1 & \underline{M}p\cos\theta_3 & \underline{M}p\cos\theta_2 & R_r + \underline{L}_r p & \underline{M}_r p & \underline{M}_r p \\ \underline{M}p\cos\theta_2 & \underline{M}p\cos\theta_1 & \underline{M}p\cos\theta_3 & \underline{M}_r p & R_r + \underline{L}_r p & \underline{M}_r p \\ \underline{M}p\cos\theta_3 & \underline{M}p\cos\theta_2 & \underline{M}p\cos\theta_1 & \underline{M}_r p & \underline{M}_r p & R_r + \underline{L}_r p \end{bmatrix} \begin{bmatrix} i_A \\ i_B \\ i_C \\ i_a \\ i_b \\ i_c \end{bmatrix} \quad (1)$$

where R_s and R_r are the resistances and L_s and L_r the self-inductances, of stator and rotor phase windings, respectively. M_s is the mutual inductance between stator phase windings, M_r the mutual inductance between rotor phase windings and M the maximum value of mutual inductance between a stator and a rotor phase winding. θ_1, θ_2 and θ_3 are the angular displacements between the axes of stator phase A and rotor phases a, b and c, respectively.

All stator/rotor mutual-inductance terms are functions of the rotor angular position and hence of time. The linear differential equations therefore do not have constant coefficients and cannot be integrated in a simple, straightforward manner and transformations must be applied to yield equations with constant coefficients. It is customary to perform two transformations in cascade.

The first is the phase transformation given by the matrix $\boldsymbol{C}_1$.

$$\boldsymbol{C}_1 = \sqrt{(2/3)}\begin{array}{c} \\ A \\ B \\ C \end{array}\begin{array}{c} \begin{array}{ccc} D & Q & 0 \end{array} \\ \begin{bmatrix} 1 & 0 & 1/\sqrt{(2)} \\ -(1/2) & \sqrt{3}/2 & 1/\sqrt{(2)} \\ -(1/2) & -\sqrt{3}/2 & 1/\sqrt{(2)} \end{bmatrix} \end{array} \tag{2}$$

whereby the three-phase stator and rotor variables are transformed to quadrature-phase variables.

The second is the commutator transformation given by matrix $\boldsymbol{C}_2$

$$\boldsymbol{C}_2 = \begin{array}{c} \\ D \\ Q \\ 0 \end{array}\begin{array}{c} \begin{array}{ccc} d & q & 0 \end{array} \\ \begin{bmatrix} \cos\theta_1 & \sin\theta_1 & 0 \\ \sin\theta_1 & -\cos\theta_1 & 0 \\ 0 & 0 & 1 \end{bmatrix} \end{array} \tag{3}$$

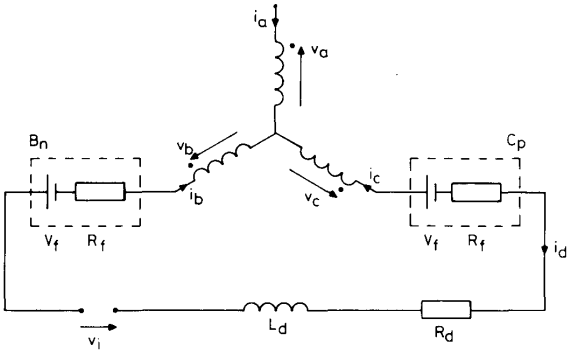

Fig. 3 *Effective rotor circuit and constraints for conduction state 1*
C_p and B_n conduct
$i_a = 0$
$i_b + i_c = 0$
$v_c - v_b - (R_d + 2R_f + L_d P)i_b - (v_l + 2v_f) = 0$

which further transforms the rotor variables on to a frame of reference which is stationary with respect to the stator.

The two transformations result in the familiar DQdq stationary-axis equation [5] widely used in the literature for analysing induction-machine behaviour under both steady-state and transient conditions.

For analysis of static Kramer operation, however, it is advantageous to retain the natural rotor variables in abc form because of their importance in determining the commutation instants and the effective rotor circuit at any time during drive operation. Eqn. 1 is thus simplified by two transformations of the stator variables only [4]. The first is the DQ-phase transformation and the second is given by the transformation matrix $\boldsymbol{C}_3$

$$\boldsymbol{C}_3 = \begin{array}{c} \\ D \\ Q \\ 0 \end{array}\begin{array}{c} \begin{array}{ccc} \Gamma & \Delta & 0 \end{array} \\ \begin{bmatrix} \cos\theta_1 & -\sin\theta_1 & 0 \\ \sin\theta_1 & \cos\theta_1 & 0 \\ 0 & 0 & 1 \end{bmatrix} \end{array} \tag{4}$$

$\boldsymbol{C}_1$ and $\boldsymbol{C}_3$ are orthogonal matrices, leading to identical transformations for currents and voltages.

Stator variables are thus transformed on to a frame of reference which is stationary with respect to the rotor, yielding the new voltage equation

$$\begin{bmatrix} v_\Gamma \\ v_\Delta \\ v_a \\ v_b \\ v_c \end{bmatrix} = \begin{bmatrix} R_s & -\omega_r L_s & 0 & -\sqrt{3}M\omega_r/2 & \sqrt{3}M\omega_r/2 \\ \omega_r L_s & R_s & \omega_r M & -M\omega_r/2 & -M\omega_r/2 \\ 0 & 0 & R_r & 0 & 0 \\ 0 & 0 & 0 & R_r & 0 \\ 0 & 0 & 0 & 0 & R_r \end{bmatrix}\begin{bmatrix} i_\Gamma \\ i_\Delta \\ i_a \\ i_b \\ i_c \end{bmatrix}$$
$$+ \begin{bmatrix} L_s & 0 & M & -M/2 & -M/2 \\ 0 & L_s & 0 & \sqrt{3}M/2 & -\sqrt{3}M/2 \\ M & 0 & L_r & 0 & 0 \\ -M/2 & \sqrt{3}M/2 & 0 & L_r & 0 \\ -M/2 & -\sqrt{3}M/2 & 0 & 0 & L_r \end{bmatrix}\begin{bmatrix} pi_\Gamma \\ pi_\Delta \\ pi_a \\ pi_b \\ pi_c \end{bmatrix} \tag{5}$$

where $L_s = \underline{L}_s - \underline{M}_s$, $L_r = \underline{L}_r - \underline{M}_r$, $M = \sqrt{(3/2)}\underline{M}$ and ω_r is the rotor angular velocity.

Note that in all forms of the static Kramer drive (three-wire fed), zero-sequence conditions cannot arise and are eliminated from eqn. 5.

v_Γ and v_Δ, the voltages in the new reference frame fixed to the rotor, are then given by

$$v_\Gamma = \sqrt{(3)}\,V_w \sin(s\omega t) \tag{6}$$

$$v_\Delta = -\sqrt{(3)}\,V_w \cos(s\omega t) \tag{7}$$

where V_w is the RMS stator phase-winding voltage.

3 Possible rotor states

In normal operation only two or three diodes conduct at any one time, diode-commutation overlap rarely extending beyond 60°. Hence there are twelve possible rotor states which may be defined by diode-conduction patterns, and one nonconducting state (state 13) in which no diode conducts, as can happen when the DC-link current becomes discontinuous. The twelve conduction states fall into two types, each repeated cyclically six times. The odd-numbered states, 1 to 11, occur when only two diodes conduct; the even-numbered, 2 to 12, when three diodes conduct, i.e. with commutation still in progress.

The effective rotor circuit during conduction state 1 is shown in Fig. 3, together with the corresponding rotor

variable constraints which allow further simplification of the system equation for that particular state.

For rotor state 1, the system equation becomes

$$\begin{bmatrix} v_\Gamma \\ v_\Delta \\ v_i + 2V_f \end{bmatrix} = \begin{bmatrix} R_s & -\omega_r L_s & -(\sqrt{3}M\omega_r) \\ \omega_r L_s & R_s & 0 \\ 0 & 0 & -(2R_r + 2R_f + R_d) \end{bmatrix} \begin{bmatrix} i_\Gamma \\ i_\Delta \\ i_b \end{bmatrix} + \begin{bmatrix} L_s & 0 & 0 \\ 0 & L_s & (\sqrt{3}M) \\ 0 & -(\sqrt{3}M) & -(2L_r + L_d) \end{bmatrix} \begin{bmatrix} pi_\Gamma \\ pi_\Delta \\ pi_b \end{bmatrix} \quad (8)$$

where V_f is the diode threshold voltage, R_f the diode slope resistance and R_d the DC-link resistance.

The system equation for rotor state 2 can be derived by applying the rotor constraints shown in Fig. 4

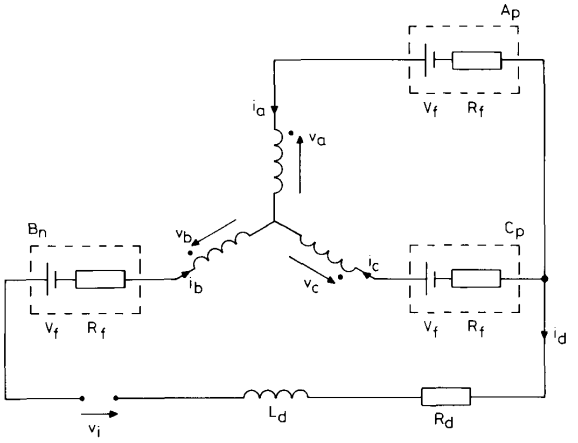

Fig. 4 *Effective rotor circuit and constraints for conduction state 2*
A_p, C_p and B_n conduct
$i_a + i_b + i_c = 0$
$(v_a - v_c) - R_f i_b - 2R_f i_c = 0$
$v_c - v_b - (R_d + R_f + L_d p)i_b + R_f i_c - (v_i + 2V_f) = 0$

$$\begin{bmatrix} v_\Gamma \\ v_\Delta \\ v_i + 2V_f \\ 0 \end{bmatrix} = \begin{bmatrix} R_s & -\omega_r L_s & -(\sqrt{3}M\omega_r/2) & (\sqrt{3}M\omega_r/2) \\ \omega_r L_s & R_s & -3M\omega_r/2 & -3M\omega_r/2 \\ 0 & 0 & -(R_r + R_f + R_d) & R_r + R_f \\ 0 & 0 & -(R_r + R_f) & -2(R_r + R_f) \end{bmatrix} \begin{bmatrix} i_\Gamma \\ i_\Delta \\ i_b \\ i_c \end{bmatrix} + \begin{bmatrix} L_s & 0 & -3M/2 & -3M/2 \\ 0 & L_s & (\sqrt{3}M/2) & -(\sqrt{3}M/2) \\ 0 & -(\sqrt{3}M) & -(L_r + L_d) & L_r \\ 3M/2 & (\sqrt{3}M/2) & -L_r & -2L_r \end{bmatrix} \begin{bmatrix} pi_\Gamma \\ pi_\Delta \\ pi_b \\ pi_c \end{bmatrix} \quad (9)$$

The system equation for each other odd-numbered state is similar to eqn. 8, for each even-numbered state it is similar to Eqn. 9, and for the nonconducting state it is obtained by omitting the last two columns and rows from eqn. 9.

4 Transitions between rotor states

The conditions for transition between one rotor state and another must be clearly defined before calculation of motor performance. Initially, no current flows and the rotor state is determined by the relative magnitudes of inverter and rotor voltages. Thereafter, transitions from one rotor state to the next depend on the type of rotor state applying at the time.

Transition from an odd-numbered to an even-numbered state occurs when a nonconducting diode becomes forward-biased, thus signalling the start of a new commutation process. The opposite transition occurs when the current in a diode falls to zero, marking the end of commutation.

Transitions from one conducting rotor state to another can only occur between numerically adjacent states, e.g. it is not possible to transfer directly from state 1 to state 3. Transitions can, however, occur from any conduction state to the nonconducting state (state 13) if the DC-link current should become zero. The nonconducting state then persists until i_d starts to flow again, whereupon the new rotor state is determined by the relative magnitudes of rotor voltages.

5 Solution of system equations

5.1 General

Operation at a given constant speed is described by a system of first-order, linear differential equations with constant coefficients. During each of the 13 distinct rotor states, the system equations can be rearranged in the form

$$pi_j = \sum_{k=1}^{n} a_{jk} i_k + h_j(t) \quad [\text{for } j = 1, 2, \ldots, n] \quad (10)$$

where a_{jk} is the element in the jth row and kth column of an $n \times n$ matrix $\boldsymbol{A}$, ($n = 3$ for states 1, 3, 5, 7, 9 and 11; $n = 4$ for states 2, 4, 6, 8, 10 and 12; $n = 2$ for state 13).

In matrix notation the system equation can be written

$$p\boldsymbol{i} = \boldsymbol{A}\boldsymbol{i} + \boldsymbol{h} \quad (11)$$

where $\boldsymbol{i}$ and $\boldsymbol{h}$ are column matrices with n elements.

Assuming that $\boldsymbol{A}$ has n linearly independent eigenvectors, $\boldsymbol{x}_1, \boldsymbol{x}_2, \ldots, \boldsymbol{x}_n$, then

$$\boldsymbol{AX} = \boldsymbol{XD} \quad (12)$$

where $\boldsymbol{X}$ is a matrix with column vectors $\boldsymbol{x}_1, \ldots, \boldsymbol{x}_n$ and $\boldsymbol{D}$ is a diagonal matrix of corresponding eigenvalues $\lambda_1, \ldots, \lambda_n$.

Matrix $\boldsymbol{X}$ can be introduced into eqn. 11 by setting

$$\boldsymbol{i} = \boldsymbol{Xz} \quad (13)$$

Then $p\boldsymbol{i} = \boldsymbol{X}p\boldsymbol{z}$ and eqn. 11 becomes $\boldsymbol{X}p\boldsymbol{z} = \boldsymbol{AXz} + \boldsymbol{h}$ which, since the columns of $\boldsymbol{X}$ are linearly independent and $\boldsymbol{X}$ is therefore nonsingular, can be rearranged as

$$p\boldsymbol{z} = \boldsymbol{Dz} + \boldsymbol{Uv} \quad (14)$$

where $\boldsymbol{v}$ is the voltage column matrix in the system equation and $\boldsymbol{U}$ is a matrix of constant coefficients given by $\boldsymbol{Uv} = \boldsymbol{X}^{-1}\boldsymbol{h}$.

In terms of its components, taking $\boldsymbol{Dz}$ to the left, eqn. 14 can be rewritten as

$$pz_j - \lambda_j z_j = r_j(t) \quad [\text{for } j = 1, \ldots, n] \quad (15)$$

where, because of the definition of matrix multiplication, $r_j(t)$ is a linear combination of $v_\Gamma(t)$, $v_\Delta(t)$ and $v_i(t)$.

The solution of eqn. 15 is given by

$$z_j(t) = e^{\lambda_j t}\left(\int e^{-\lambda_j t} r_j(t)\, dt + c_j\right) \quad (16)$$

where c_j is an arbitrary constant of integration, the value of which may be obtained by solving the initial condition $\boldsymbol{i}(t_o) = \boldsymbol{i}_o$. $\boldsymbol{z}_o$ can then be determined from

$$\boldsymbol{z}(t_o) = \boldsymbol{z}_o = \boldsymbol{X}^{-1}\boldsymbol{i}_o \tag{17}$$

5.2 Application to constant-speed drive operation

For a given constant speed, the elements of $\boldsymbol{A}$, its eigenvalues and corresponding eigenvectors are constants, and the functions $r_j(t)$ are given by a linear combination, with constant coefficients, of the n elements of the voltage column matrix $\boldsymbol{v}$ in the system equation for that rotor state. A unique solution $\boldsymbol{i}(t)$ of the initial value problem can thus be obtained for the time interval in which $\boldsymbol{v}(t)$ is continuous. This involves obtaining an analytical solution of eqn. 16 and the assignment of the appropriate value to c_j, which is necessary whenever a change of rotor state or a discontinuity in v_i is detected.

Ignoring supply-impedance effects, the inverter DC voltage v_i can be written as

$$v_i = N[Av_{AB} + Bv_{BC} + Cv_{CA}] + 2V_t \tag{18}$$

where v_{AB}, v_{BC} and v_{CA} are suppply line-to-line voltages and N is the recovery-transformer voltage ratio. A, B and C are switching functions whose values at any instant depend on the value of firing-delay angle. V_t is the thyristor threshold voltage. The inverter-thyristor resistance drops are allowed for in the analysis by incorporating $(2R_t)$ into the DC-link-resistance term R_d.

Eqn. 16 can be rewritten as

$$z_j = e^{\lambda_j t}\left(c_j + U_{j1}\int e^{-\lambda_j t}v_\Gamma\,dt + U_{j2}\int e^{-\lambda_j t}v_\Delta\,dt + U_{j3}\int e^{-\lambda_j t}(v_i + 2V_f)\,dt\right) \tag{19}$$

Note that the terms involving U_{j3} and v_i disappear when the rotor is in the nonconducting state.

Substituting for v_Γ and v_Δ

$$\int e^{-\lambda_j t}v_\Gamma\,dt = -\sqrt{(3)}\,V_w\{e^{-\lambda_j t}/[(s\omega)^2 + (\lambda_j)^2]\} \times [(s\omega)\cos(s\omega t) + \lambda_j \sin(s\omega t)] \tag{20}$$

and

$$\int e^{-\lambda_j t}v_\Delta\,dt = -\sqrt{(3)}\,V_w\{e^{-\lambda_j t}/[(s\omega)^2 + (\lambda_j)^2]\} \times [(s\omega)\sin(s\omega t) - \lambda_j \cos(s\omega t)] \tag{21}$$

Substituting for v_i, the third integral in eqn. 19 can be obtained

$$\begin{aligned}\int e^{-\lambda_j t}(v_i + 2V_f)\,dt &= \sqrt{(6)}(NV_w)\{e^{-\lambda_j t}/[\omega^2 + \lambda_j^2]\} \\ &\times \{A[\omega\cos(\omega t + \Phi) + \lambda_j \sin(\omega t + \Phi)] \\ &+ B[\omega\cos(\omega t + \Phi - 2\pi/3) \\ &+ \lambda_j \sin(\omega t + \Phi - 2\pi/3)] \\ &+ C[\omega\cos(\omega t + \Phi - 4\pi/3) \\ &+ \lambda_j \sin(\omega t + \Phi - 4\pi/3)]\} \\ &- (2V_f + 2V_t)e^{-\lambda_j t}/\lambda_j\end{aligned} \tag{22}$$

where Φ is 0 or $\pi/6$ depending on whether the stator is connected in delta or star, respectively.

System equations are thus solved for i_Γ, i_Δ, i_a, i_b, i_c and their derivatives. All other quantities of interest such as stator currents, rotor phase and line voltages, DC-link current, recovery-transformer currents and AC-supply currents can then be obtained.

The instantaneous torque developed by the machine is given by

$$T = p\{i_\Gamma[-L_s i_\Delta - \sqrt{3}\,M(i_b - i_c)/2] + i_\Delta[L_s i_\Gamma + Mi_a - M(i_a - M(i_b + i_c)/2]\} \tag{23}$$

where p is the number of pole-pairs.

6 Computation of performance

The analysis described above was incorporated in a computer program which calculates drive performance in terms of the machine ABCabc voltages and currents, supply currents, supply and stator instantaneous power flow, DC-link-current and -voltage waveforms, torque developed by the machine, etc. The eigenvalues λ_j and the corresponding eigenvectors $\boldsymbol{x}_j$ are evaluated numerically, once for each rotor state, using NAG library subroutines. The operation of the program is outlined in the flowchart shown in Fig. 5.

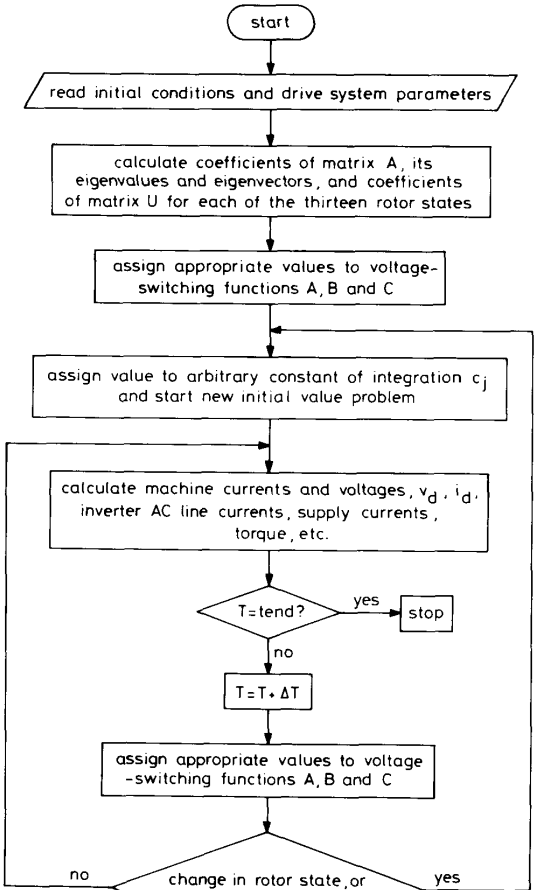

Fig. 5 *Flowchart of drive steady-state simulation program*

7 Computed and measured waveforms

7.1 General

The simulation program has been verified for a variety of practical conditions. Computed and practical waveforms are compared side-by-side, and show the degree to which complicated drive waveforms can be accurately predicted by the analysis.

A 7.5-kW, 415-V, four-pole, 50-Hz motor was used for the experimental investigation and representative results are shown below for three constant speeds, each chosen to highlight a particular feature of drive behaviour.

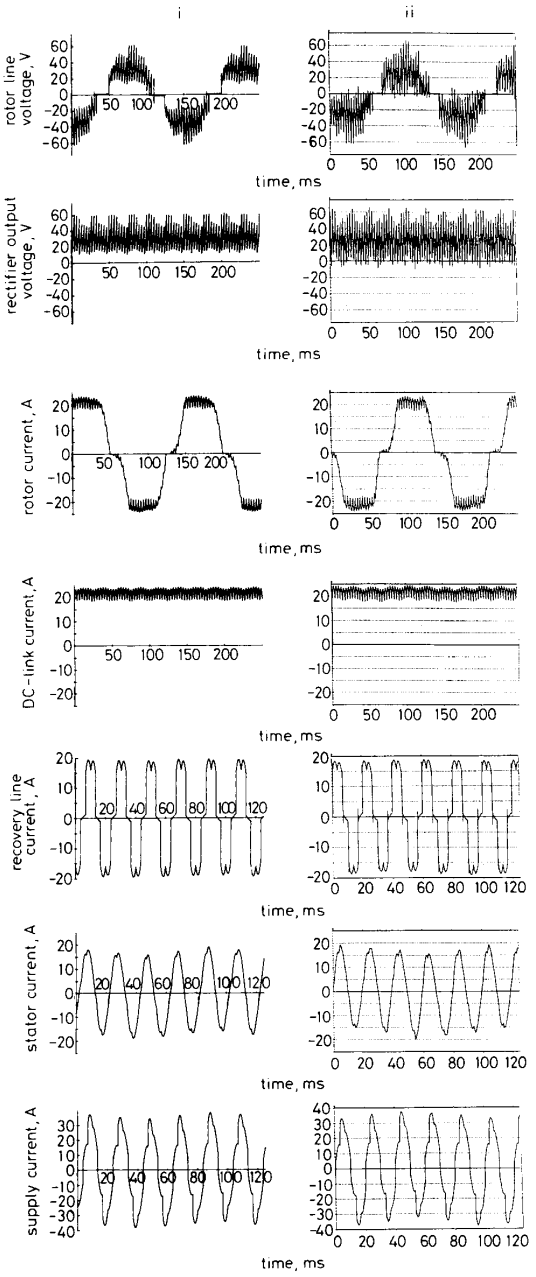

Fig. 6 *Drive waveforms at 1300 rev/min with a DC-link current of 22 A mean*

i Predicted
ii Measured

Machine and circuit parameters are listed in the Appendix.

7.2 Operation at 1300 rev/min

Fig. 6 shows waveforms for a speed of 1300 rev/min (slip = 0.1333) and mean DC-link current I_d of 22 A, for which $\alpha = 92.8°$.

The rotor line-to-line voltage shows very clearly the periods of rectifier overlap during which the lines are short-circuited by two conducting diodes. The waveform includes spikes, at six times supply frequency, caused by the step changes in inverter input voltage, which are present at all speeds but more apparent at high speeds where the fundamental rotor voltage is small. The measured results clearly contain high-frequency ringing not shown in the predicted waveforms.

The DC-link-current waveform shows very clearly the ripple components (*a*) at six times supply frequency caused by the inverter input voltage (*b*) at six times rotor frequency due to diode rectifier output voltage. These also appear, modulated at low slip frequency, in the rotor-current waveform which is of the familiar shape and shows the gradual rise and fall during rectifier overlap.

Because of the DC-link-current ripple, diode commutation is clearly not completed in one continuous stage. Instead, at the low levels of current at the start of commutation, the rotor-conduction state may alternate between even- and odd-numbered states, e.g. the sequence may be 12-1-2-1-2-1-2-3.

The recovery line current comprises 120°-wide pulses of DC-link current, in addition to the transformer-magnetising current. The stator current is then added to give the total supply current. Pulsations in stator and supply-current waveforms, caused by the reflection of rotor harmonics into the stator (see Section 10), are clearly visible.

7.3 Operation at 975 rev/min

Fig. 7 shows waveforms ($\alpha = 102.6°$) for a speed of 975 rev/min (slip = 0.35) and a mean DC-link current of 12 A. The waveforms show very clearly the typical characteristics associated with static Kramer operation; for example, the effects of commutation overlap are clearly visible in the rotor line voltage and at the rising and falling edges of the rectangular rotor-current waveform.

Of particular interest, however, is the cyclic variation of stator and supply RMS currents which becomes very apparent at speeds near 1000 rev/min (slip of 1/3). Because it occurs at a frequency and magnitude to which measuring instruments can respond, the fluctuation occasionally causes some anxiety amongst drive users. The origins of these effects are discussed further in Section 10.

7.4 Operation at 550 rev/min

The torque, and hence current, required at low speeds for a fan-type load is small and the DC-link current can become discontinuous. Such a condition is examined here.

Fig. 8 shows waveforms for a speed of 550 rev/min (slip = 0.633) with a DC-link current of only 1.6 A ($\alpha = 120.1°$). The effects of discontinuous current upon rotor and recovery line-current waveforms are obvious, as is the contribution of transformer current to recovery line current.

The rotor-voltage waveforms are shown together with rectifier output voltage, the latter highlighting those periods when i_d is zero and the diodes do not conduct,

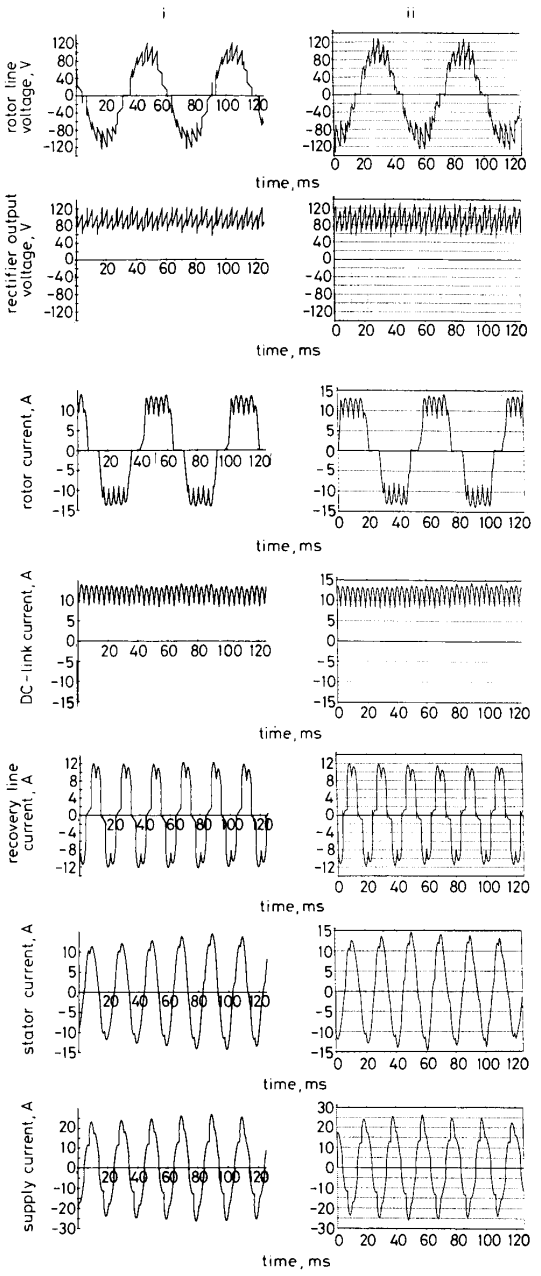

Fig. 7 *Drive waveforms at 975 rev/min with a DC-link current of 12 A mean*
i Predicted
ii Measured

7.5 Computed and measured torque waveforms

Fig. 9 shows computed electromagnetic-torque and measured shaft-torque waveforms for the first two conditions

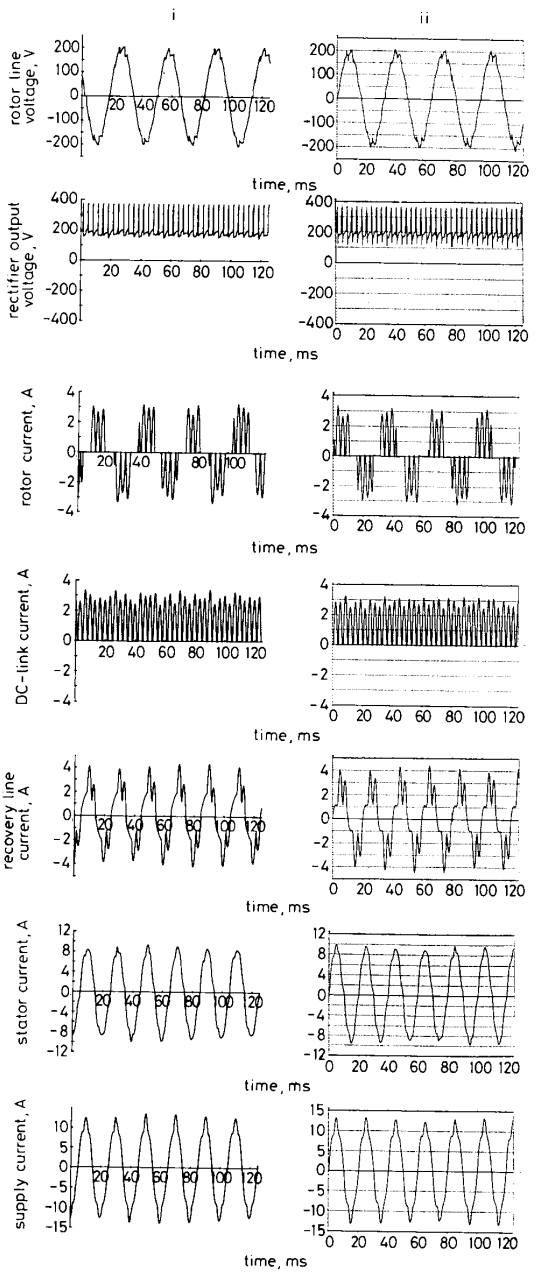

Fig. 8 *Drive waveforms at 550 rev/min with a discontinuous DC-link current of only 1.6 A mean*
i Predicted
ii Measured

giving the voltage spikes which are so evident in its waveform. (Strictly speaking, v_d is undefined when i_d is zero because neither thyristors nor diodes then conduct, but in practice v_d follows the inverter back EMF, presumably due to the low leakage resistances of thyristors which are being fired.)

mentioned above. The measured shaft-torque waveforms do not show the predicted high-frequency pulsations caused by inverter switching, but otherwise the two sets of waveforms correspond well.

Although Fig. 9*a* displays torque pulsations at six times rotor frequency caused by nonsinusoidal machine-

current waveforms (see Section 9) and which could cause trouble if their frequency coincided with a natural,

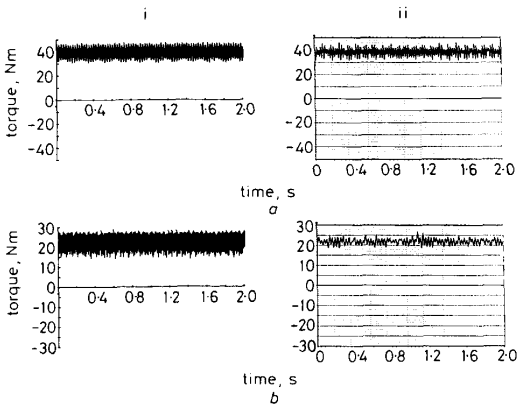

Fig. 9 *Torque waveforms*
i Predicted
ii Measured
a 1300 rev/min
b 975 rev/min

mechanical resonance frequency of the system, the torque waveforms show an absence of low-frequency pulsations which might correspond to the stator-current pulsations seen earlier.

8 Frequency spectrum calculations

Harmonic currents are inevitably injected into the supply due to the switching action of the inverter bridge. In addition, rotor-current harmonics are produced by the rectifier at frequencies which are integer multiples of slip frequency. These harmonics are reflected into the stator windings and fed into the mains at frequencies given by

$$f_{(stator)} = f(1 \pm 6ks) \tag{24}$$

where f is mains frequency, s is p.u. slip and $k = 1, 2, 3$ etc. (negative values correspond to negative-sequence rotor-current harmonics).

Some effects of these harmonic fields, such as machine-locking torques, have been highlighted in the literature [6], and others, i.e. torque- and stator-current pulsations [7, 8], have already been mentioned. A full investigation of the effects of these harmonics is beyond the scope of this paper but it will be seen that the computed and measured values agree well, showing that their magnitudes can be accurately predicted.

Figs. 10 and 11 show the frequency spectra of simulated and measured recovery, stator and overall supply-current waveforms for the first two conditions mentioned above. In addition to the 5th, 7th, 11th and 13th harmonic components of the recovery line currents, subharmonics at frequencies given by eqn. 24 are introduced into the stator-current waveform. The overall supply-current spectrum then contains both stator- and recovery-circuit harmonic components.

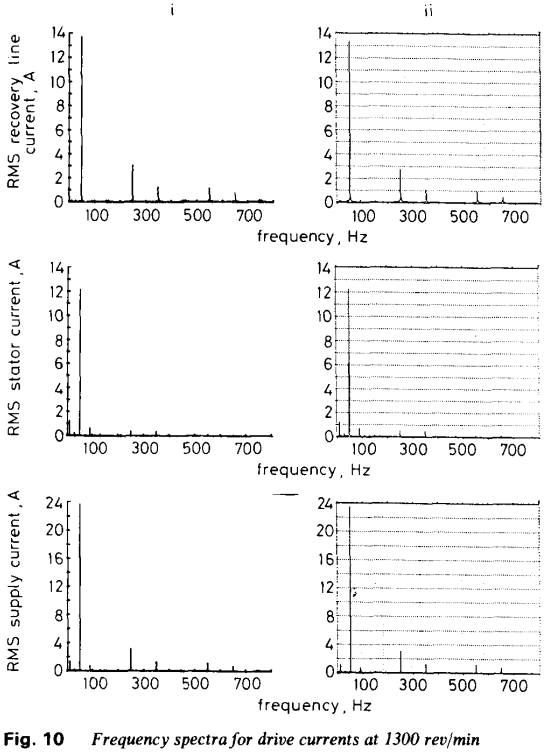

Fig. 10 *Frequency spectra for drive currents at 1300 rev/min*
i Calculated
ii Measured

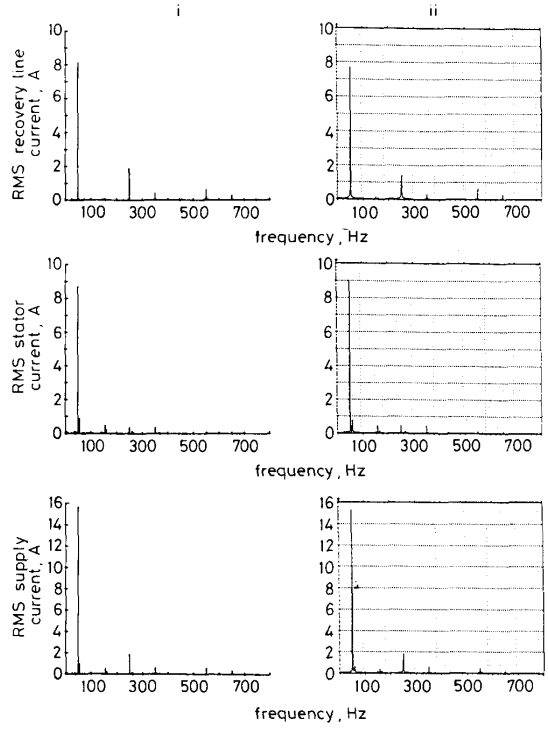

Fig. 11 *Frequency spectra for drive currents at 975 rev/min*
i Calculated
ii Measured

9 Torque pulsations at six times rotor frequency

Electromagnetic torque can be considered as the result of interaction between stator and rotor MMF vectors, $\boldsymbol{F}_s$ and $\boldsymbol{F}_r$, respectively. Torque is then proportional to $(\boldsymbol{F}_s \boldsymbol{F}_r \sin \psi_{sr})$, where ψ_{sr} is the angle between $\boldsymbol{F}_s$ and $\boldsymbol{F}_r$ at any instant.

A steady torque can only be produced by interaction between components of F_s and F_r having a common angular speed: only then can the angle ψ_{sr} remain constant. Torque pulsations occur, however, when ψ_{sr} varies, the rate of change being controlled by the difference between the angular speeds of the F_s and F_r components [9].

In a static Kramer drive, the order of the three most significant rotor-current harmonics, together with the angular speed of their MMF vectors and the frequency of the induced stator currents (calculated from eqn. 24), are listed in Table 1.

Table 1: Effects of rotor harmonics and slip

Order of rotor harmonic	Rotating speed of rotor MMF	Frequency of induced stator current
1	ω	f
5	$(1-6s)\omega$	$f-6sf$
7	$(1+6s)\omega$	$f+6sf$

Clearly, as a result of the interaction between the various harmonic MMF vectors, the electromagnetic-torque waveform must include pulsations at a frequency given by $(6sf)$.

10 Stator-current pulsations

If the stator current comtains sideband harmonic components whose frequencies approach that of the mains, the amplitudes of stator and supply currents become modulated at low frequency given by the difference between the harmonic-stator current and supply frequency. This beat effect is very clearly visible in Figs. 12 and 13, which show predicted stator current and torque waveforms for operation at 1360 and 960 rev/min, respectively, together with the stator-current harmonic content.

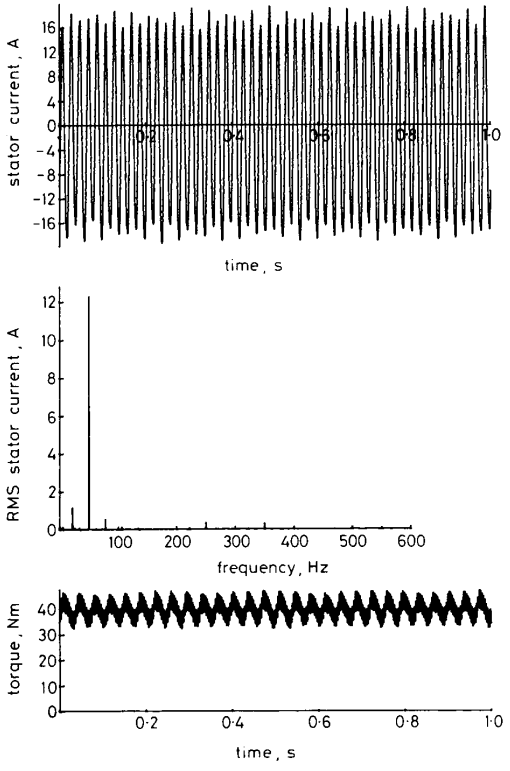

Fig. 12 *Predicted stator-current waveform and frequency spectrum and torque waveform at 1360 rev/min*

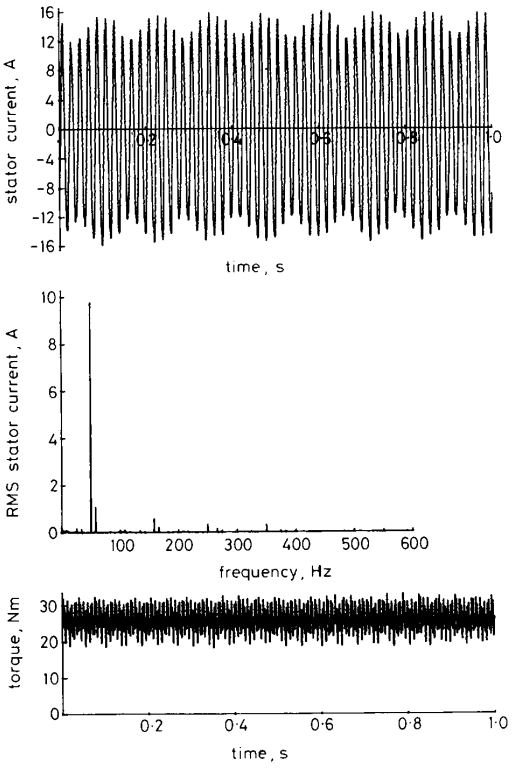

Fig. 13 *Predicted stator-current waveform and frequency spectrum and torque waveform at 960 rev/min*

The sideband harmonics contained in the stator-current frequency spectrum at frequencies given by eqn. 24 are clearly shown, and although the amplitude of stator current is modulated, very little effect is visible in the torque waveforms, indicating that the current pulsations do not cause or imply large torque oscillations.

It should perhaps be noted that pulsating-current waveforms are very similar to an amplitude-modulated wave. Neglecting higher harmonic components, $i(t)$ could be written as

$$i(t) = A\cos(\omega t) + B\cos[(\omega+\omega_1)t] + C\cos[(\omega-\omega_2)t] \quad (25)$$

i.e. a fundamental component of amplitude A, an upper sideband (if present) of amplitude B and a lower sideband (if present) of amplitude C.

At p.u. slips of 1/3, 1/6, 1/9, etc., the negative-sequence currents produced by rotor 5th, 11th and 17th harmonics, respectively, will produce unequal currents in each stator phase. The induced stator harmonics then occur at integer multiples of supply frequency and cause no stator-current pulsations. This is clearly demonstrated in Fig. 14 which shows stator- and rotor-current waveforms and their harmonic content, together with the electromagnetic-torque waveform at 1250 rev/min (slip = 1/6).

These waveforms were calculated for a modified Kramer system in which the recovery inverter has been replaced by a DC machine so that v_i becomes simply a

constant DC-voltage V_i. The high-frequency torque-ripple content, due to inverter-switching operation, has

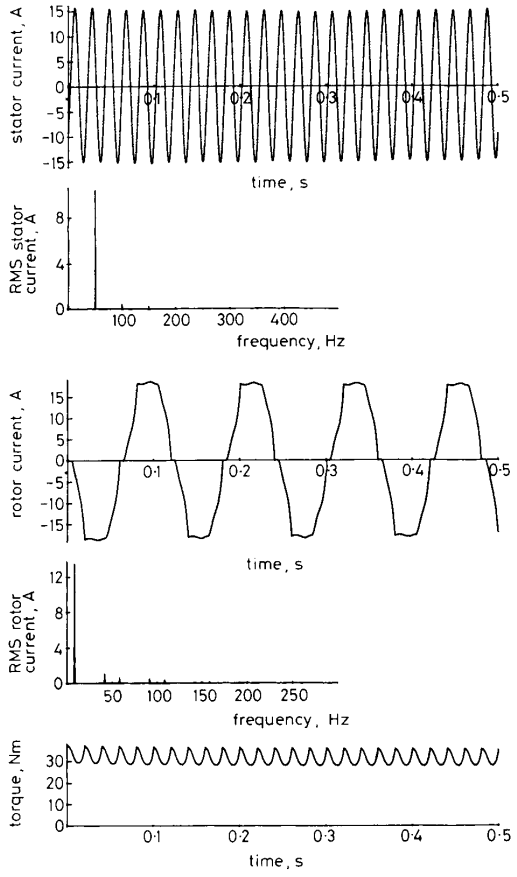

Fig. 14 *Predicted stator-current waveform and frequency spectrum rotor-current waveform and frequency spectrum and torque waveform at 1250 rev/min for modified Kramer drive*

disappeared (but not the low-frequency ripple at six times rotor frequency). Note that the rotor-current waveform at this speed (slip = 1/6) differs markedly from that shown in Fig. 6 for 1300 rev/min. Commutation overlap has become extended and the 5th harmonic component is very low, exactly as predicted by Kleinrath [7].

11 Conclusions

A computer model, based on steady-state eigenvalue and eigenvector solution of machine equations, offers a fast method for the simulation, analysis and performance determination of a static Kramer drive under practical operating conditions.

The analysis is based on a transformation, of stator variables only, on to a reference frame which is stationary with respect to the rotor, thus eliminating time-varying functions of rotor angle from the machine-voltage equation. Natural rotor variables are retained because of their importance in defining diode-conduction states and the corresponding rotor-circuit constraints. The time-varying inverter DC-voltage can then be introduced into the system equation which can still be integrated in a simple manner.

The analysis has been verified by comparison of simulated and measured waveforms and used to investigate the phenomenon of pulsating stator and supply currents at certain speeds which were found to be independent of machine-torque pulsations. The results confirm that despite both being caused by nonsinusoidal machine currents, stator-current pulsations do not cause, nor are they caused by, machine-torque pulsations and *vice versa*.

Compared with the numerical solution [4] of eqn. 5, the method described in this paper gives improved accuracy and a nine-fold reduction in the CPU time required for computation of drive performance.

12 Acknowledgments

The authors wish to acknowledge support received from the Science and Engineering Research Council, the Committee of Vice Chancellors and Principals and the University of Newcastle upon Tyne where the work was carried out.

13 References

1 GIANNAKOPOULOS, G., and GALANOS, S.: 'Dynamic simulation of an induction motor drive with DC link in the rotor circuit'. IEEE Power Engineering Society, Winter Meeting, New York, USA, 1979, Paper A79, pp. 112–14
2 FRANZ, P., and MEYER, A.: 'Digital simulation of a complete subsynchronous convertor cascade with 6/12-pulse feedback system', *Trans. IEEE*, 1981, **PAS-100,** (12), pp. 4948–4957
3 HUBER, G.N.: 'Digital simulation of the asynchronous cascade with semiconductor rectifiers'. Proceedings of International Conference on Electrical Machines, Brussels, Belgium, 1978, **II,** pp. E3.6/1–10
4 BROWN, J.E., DRURY, W., JONES, B.L., and VAS, P.: 'Analysis of the periodic transient state of a static Kramer drive', *IEE Proc. B*, 1986, **133,** (1), pp. 21–30
5 JONES, C.V.: 'The unified theory of electrical machines' (Butterworths, London, 1967)
6 BLAND, R.J., HANCOCK, N.N., and WHITEHEAD, R.W.: 'Considerations concerning a modified Kramer system', *Proc. IEE*, 1963, **110,** (12), pp. 2228–2232
7 KLEINRATH, H.F.: 'Torque pulsation of an induction motor with speed control by a static frequency changer in the slip ring circuit'. Proceedings of International Conference on Electrical Machines, Brussels, Belgium, 1978, **II,** pp. E3.8/1–9
8 LABER, H.: 'Subsynchronous static converter cascades with reduced effect on the system and increased reliability', *Siemens Power Eng.*, 1979, **1,** (12), pp. 384–387
9 ROBERTSON, S.D.T., and HEBBAR, K.M.: 'Torque pulsations in induction motors with inverter drives', *Trans. IEEE*, 1971, **IGA-7,** (2), pp. 318–323

14 Appendix

14.1 Induction-motor equivalent-circuit parameters

The star-equivalent, per-phase parameters of the equivalent circuit of the test motor used in the investigation were as follows:

$R_1 = 0.475\ \Omega$ (stator resistance)

$X_1 = 1.597\ \Omega$ (stator leakage reactance)

$X_m = 36.94\ \Omega$ (magnetising reactance)

$X'_2 = 1.597\ \Omega$ (rotor leakage reactance, referred to stator)

$R'_2 = 0.634\ \Omega$ (rotor resistance, referred to stator)

$n = 0.553$ (rotor/stator turns ratio)

The parameters of the $\Gamma\Delta$abc machine equation used in the analysis are not in a form which relates directly to

these equivalent circuit parameters. However, the two sets of parameters can be simply related as follows:

$$R_s = R_1 \tag{26}$$

$$L_s = (X_1 + X_m)/\omega \tag{27}$$

$$M = n\sqrt{(2/3)}X_m/\omega \tag{28}$$

$$R_r = n^2 R'_2 \tag{29}$$

$$L_r = n^2(X'_2 + X_m)/\omega \tag{30}$$

14.2 Recovery circuit parameters

Diodes: $V_f = 0.8$ V, $R_f = 8$ mΩ

DC link: $L_d = 34$ mH, $R_d = 0.2$ Ω

Thyristors: $V_t = 1.2$ V, $R_t = 9$ mΩ

Recovery-transformer turns ratio $N = 0.7333$